Effects of strain and trapping on hydrogen-induced cracking in high strength low alloy steels

Cédric Bosch, David Delafosse, Xavier Longaygue

▶ **To cite this version:**

Cédric Bosch, David Delafosse, Xavier Longaygue. Effects of strain and trapping on hydrogen-induced cracking in high strength low alloy steels. European Corrosion Congress 2010 (Eurocorr 2010), Sep 2010, Moscou, Russia. pp.1558-1570. emse-01063599

HAL Id: emse-01063599

https://hal-emse.ccsd.cnrs.fr/emse-01063599

Submitted on 12 Sep 2014

HAL is a multi-disciplinary open access archive for the deposit and dissemination of scientific research documents, whether they are published or not. The documents may come from teaching and research institutions in France or abroad, or from public or private research centers.

L'archive ouverte pluridisciplinaire **HAL**, est destinée au dépôt et à la diffusion de documents scientifiques de niveau recherche, publiés ou non, émanant des établissements d'enseignement et de recherche français ou étrangers, des laboratoires publics ou privés.

Effects of strain and trapping on hydrogen-induced cracking in high strength low alloy steels

C. Bosch[1], *D. Delafosse*[1], *X. Longaygue*[2]
[1] *Ecole des Mines de Saint-Etienne, UMR CNRS 5146, Saint-Etienne, France;*
[2] *IFP, Rueil-Malmaison, France;*
e-mail: *bosch@emse.fr*

Summary

In pearlitic steels, trapping at interphase boundaries may induce hydrogen-cracking in the absence of applied stress such as in blistering and Hydrogen Induced Cracking. However, in low alloy steels containing a much lower amount of such trapping sites and/or when hydrogen activity is reduced, most instances of hydrogen-induced cracking involve strong interactions between local plasticity and hydrogen effects.
We investigated the effects of these variables on the crack growth rate in two quenched and tempered high strength low alloy (HSLA) steels. Slow strain rate tensile and low-amplitude cyclic tests were conducted on micro-notched specimen in conditions of variable hydrogen activity. The results indicate a strong dependence of crack growth rate with the tempering on the one hand and both the notch-tip plastic zone and hydrogen activity on the other. At low activity, dynamic strain seems to be the major factor affecting hydrogen embrittlement, while trapping effects appear dominant at higher hydrogen activity.

1 Introduction

It is well known that high strength steels are susceptible to hydrogen embrittlement (HE) and the susceptibility increases with the strength level [1]. Over the years a number of theories have been developed to explain the mechanism of hydrogen embrittlement (the hydrogen phase change theory, the pressure theory, the decohesion theory, the hydrogen enhanced local plasticity theory) [2], but none of them can explain alone the embrittling effect of hydrogen on all metals plus environments. Hydrogen embrittlement generally requires localization of hydrogen atoms at microstructural heterogeneities (interphase boundaries, precipitates, dislocations …). In environmental conditions highly hydrogenating, trapping at these sites may induce hydrogen-cracking even in the absence of applied external stress such as in blistering and Hydrogen Induced Cracking in pearlitic steels. When hydrogen activity is reduced, and/or in low alloy steels containing a much lower amount of such trapping sites, most instances of hydrogen-induced cracking involve strong interactions between local plasticity and hydrogen effects. In these conditions, hydrogen embrittlement requires additional effects to localize and increase hydrogen content at trap sites. Hydrogen trapping in plastic strain zone at crack tip and effect of hydrostatic stress on the chemical potential are important factors of localization of hydrogen. Gao *et al*. [3] investigated the hydrogen distribution around a crack tip in a low alloy steel. They showed peaks of concentration at the crack tip corresponding on one hand to the location of the maximum equivalent strain in the vicinity of the

crack tip, and on the other hand to the location of the maximum hydrostatic stress, ahead of the crack tip. In addition, experiments of hydrogen embrittlement carried out in mode III by Green *et al.* [4] and Swanson *et al.* [5] give the results of very slight embrittlement, due to the fact that hydrostatic stress is minimum and equivalent stress is maximum in these experiments. Hydrogen embrittlement is also strain rate dependant, as shown by tensile tests. These tests show a decreasing strain at fracture with decreasing loading rate, see for example Maier *et al.* [6]. Furthermore, Takai *et al.* showed that lattice defects formation (vacancies and their clusters) formed during dynamic strain with hydrogen are the most important factor causing hydrogen embrittlement [7].

The objective of this work was to investigate the effects of these variables: stress, dynamic strain and hydrogen activity, on the crack growth rate in a high strength low alloy (HSLA) steel quenched and tempered at two different temperatures. Slow strain rate tensile and low-amplitude cyclic tests were conducted on micro-notched specimen in conditions of variable hydrogen activity.

2 Experimental procedure

2.1 Materials

The investigations were carried out on low alloy steel 32C1 (0.32 C, 0.347 Cr, 0.743 Mn, 0.201 Si, 0.046 Cu, 0.016 Mo, 0.047 Ni, 0.013 Al, 0.007 P, 0.002 S) quenched and tempered at two different temperatures (designed steel A and steel B). Their mechanical properties are shown in table 1.
The steels have a tempered martensite microstructure (fig. 1), consisting of martensite laths with cementite distributed within and along lath boundaries and prior austenite grain boundaries [8-9]. It is noted that steel A is not sensitive to sulphide stress cracking (SSC) according to NACE Standard Tensile Test TM0177-96 at pH 4.5 and 1 bar H_2S environmental conditions, while steel B is SSC sensitive.

Table 1: Mechanical properties of the two steels.

	YS (MPa)	UTS (MPa)	Elongation (%)	HRC
Steel A	695	795	20.6	22
Steel B	860	935	18.6	27

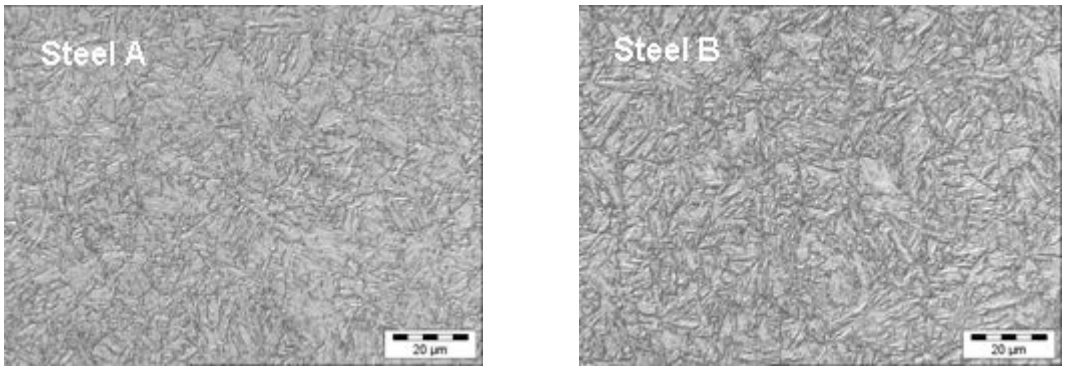

Figure 1: Microstructure of steels (tempered martensite).

2.2 Specimens

The geometry and dimensions of specimens are shown in figure 2. A micro-notch was located on one side of specimen halfway up of the gauge length, with a constant notch root radius of 40 µm and a depth between 0 (for smooth specimen) and about 300 µm. Machining was slowly performed using a precision saw wire in order to minimise local strain hardening at the notch tip. The aim is to provide a localised plastic zone that would trigger local hydrogen–deformation interactions mechanisms and cause early crack initiation under various loading and stress triaxiality conditions.

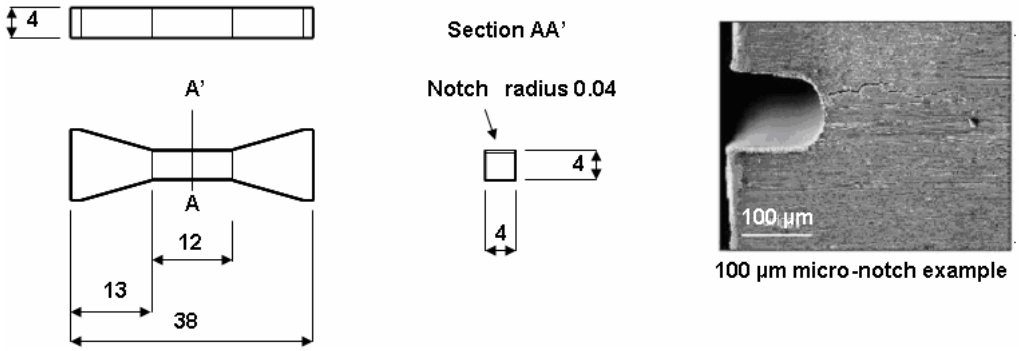

Figure 2: Specimen dimensions and example of a 0.1 micro-notch.

2.3 Test environments

Tests were performed at ambient temperature. The environmental conditions were adjusted to decrease or increase hydrogen activity on the specimens:

- for low to moderate hydrogen activity conditions: cathodic polarization of specimen at Ec=-900 mV/SCE and Ec=-1170 mV/SCE, in a 3 wt% NaCl de-aerated solution, acidified with a CO_2 gas bubbling and buffered at 3.5 pH with acetic acid.
- for high hydrogen activity conditions: cathodic polarization of specimen at Ec=-1300 mV/SCE, in an alkaline solution of 0.1 M of NaOH with 0.02 M of Na_2S. These last conditions are similar to those in a solution at 4.5 pH and 1 bar H_2S partial pressure, in terms of hydrogen permeation flux through a diaphragm of Armco iron.

2.4 Mechanical tests

Slow strain rate tensile tests (SSRTs) were performed at two strain rates: 10^{-6} s^{-1} and 10^{-7} s^{-1}. The micro-notch depths investigated in SSRTs were ranged from 0 to 300 µm.

Low-amplitude cyclic tests were performed at a fixed micro-notch of about 230 µm deep. They were conducted at load ratios R = 0.5 and R = 0.6, and a frequency of 5.10^{-3} Hz. The applied maximum load σ_{max} was ranged from 50% to 110% of the yield stress of the steels. These tests have been conducted until 3000 cycles if the samples do not broke.

2.5 Tests analysis

Stress *vs* strain plots were analyzed in terms of reduction of tensile properties according to notch depth, and compared with tensile properties of steels in air. The fracture stress was defined as the maximum load divided by the initial minimum cross section area, which was calculated as follows:

$$\sigma_F = \frac{F_{max}}{A_{min}}$$

where F_{max} is the maximum tensile load and A_{min} the initial cross section area for smooth specimens or the initial cross section net area of the micro-notch for notched specimens.
A very precise fracture surface analysis using a scanning electron microscope was performed on the broken specimens, or else on metallographic slices on unbroken ones, to measure brittle crack length and calculate the mean crack growth rate by the following equation:

$$\frac{da}{dt} = \frac{S_a}{B} \times \frac{1}{\left(t_{\sigma F} - t_0\right)}$$

where S_a is the brittle fracture surface, B is the specimen thickness, t_0 and $t_{\sigma F}$ are the initial time and the testing time to the fracture stress.
Low-amplitude cyclic tests were analyzed according to the load ratio and the applied maximum load. Mean crack growth rates have been evaluated in the same way.

3 Experimental results

3.1 Slow strain rate tests

Figure 3 shows the yield stress and fracture stress for steels A and B, determined from the stress *vs* elongation curves of SSRTs in air and in 3wt% NaCl solution. The difference between the yield stress and the fracture stress shows a general yielding before fracture whatever the depth of the notch in these environmental conditions. However, the decrease of the fracture stress with the micro-notch depth, while the yield stress remains constant, indicates that the behaviour of steels may be full brittle for a notch of about 600 µm deep for steel A, and 450 µm deep for steel B, corresponding to an elastic stress concentration factor respectively equal to 7.5 and 6.5 [10]. On the contrary, in air there is no notch effect on the behaviour of the steels, at least up to a notch of 100 µm deep. This indicates the embrittling effect of hydrogen in the steels. Crack initiation occurred early during the tensile tests, evidenced by the yield stress in air always higher than in solution.
The variation of ultimate elongation with micro-notch depth is shown in figure 4. For steel A, the elongation decreases more weakly from about 10% to 5% for micro-notch 10 µm to 170 µm deep respectively, while elongation for steel B drops to 5% for a notch less than 100 µm deep. Effect of strain rate and two hydrogenation conditions have been explored for a notch of 100 µm deep. With decreasing the strain rate, elongation decreased whatever the cathodic potential applied. Similarly, for a given strain rate a higher cathodic potential caused a lower ultimate elongation.
Fig. 5 shows the fracture surface of steel A in solution at -1170 mV/SCE and 10^{-6} s^{-1}. The general view at low magnification shows the three typical areas of the cracking observed on all specimens. At the notch root, the crack initiated and propagated in a brittle mode by quasi-cleavage. Then a ductile fracture mode gradually took place up to the final tearing. This change of fracture mode occurred at the apparent tensile strength during tensile test, which is designed fracture stress.
Figure 6 shows the fracture surfaces of steel B for all the test conditions. The crack also initiated in the vicinity of the notch root in a brittle mode, but for the lowest strain rate and the highest cathodic potential, a mixed mode intergranular and transgranular appeared.
In given test conditions, the crack length measured on fracture surfaces depended on micro-notch depth. Figure 7 shows the CGRs in 3wt% NaCl solution at -1170 mV/SCE

and 10^{-6} s^{-1} for the two steels. For small micro-notch depths, the crack growth rates of both steels are almost similar, in a scatter band around 8.10^{-9} – 2.10^{-8} m/s. Beyond 100 µm deep, CGRs reached a plateau for both steels but at a different level, indicating a highest sensitivity to hydrogen embrittlement for steel B. On the plateau, CGRs were twice as great for steel B.

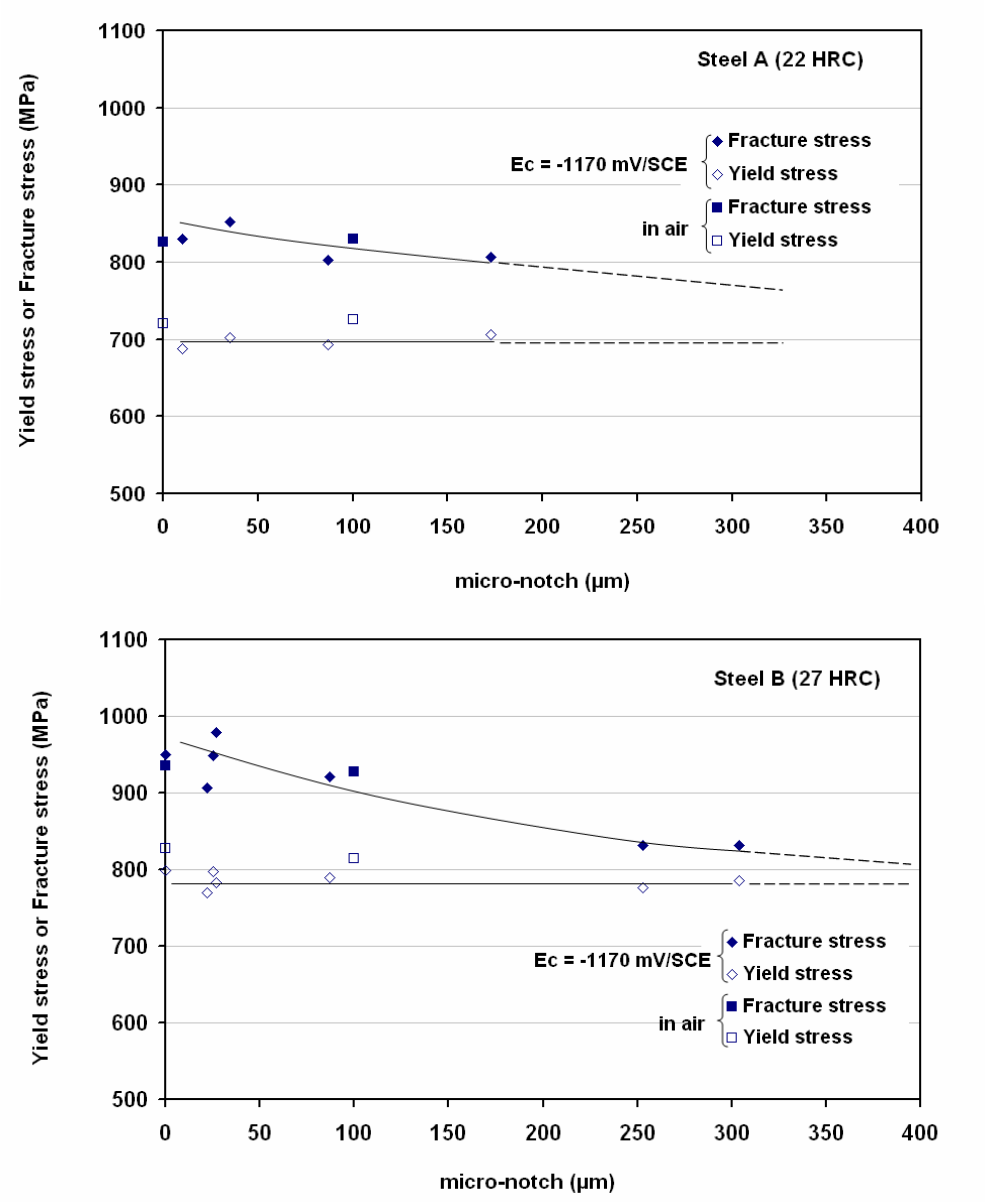

Figure 3: Plot of fracture stress *vs* micro-notch depth for steels A and B, in air and in 3 wt% NaCl de-aerated solution at Ec = -1170 mV/SCE. SSRTs at $\dot{\varepsilon}=10^{-6}$ s^{-1}.

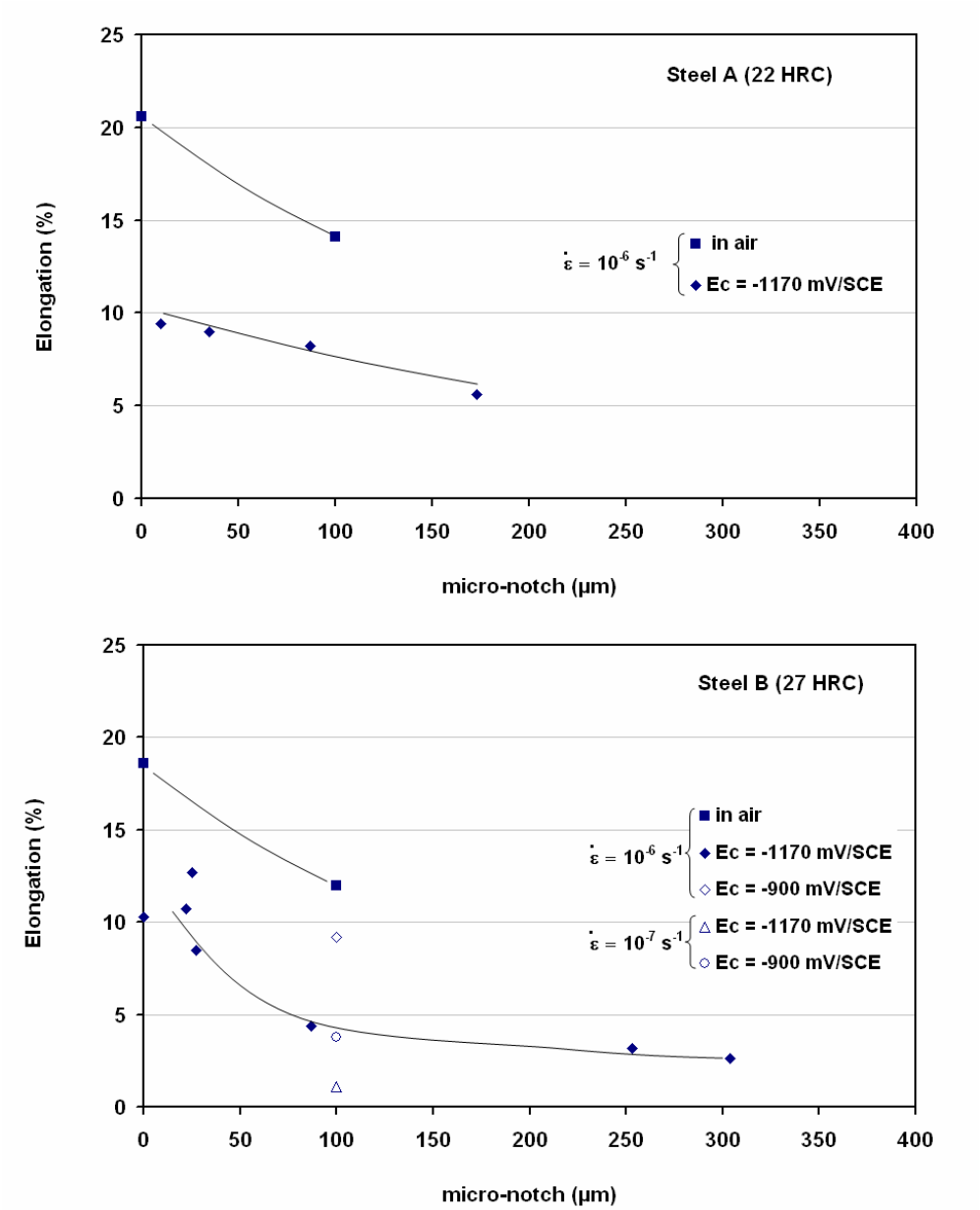

Figure 4: Plot of elongation *vs* micro-notch depth for steels A and B, in air and in 3 wt% NaCl de-aerated solution at Ec = -1170 and -900 mV/SCE. SSRTs at $\dot{\varepsilon}$ =10^{-6} and 10^{-7} s^{-1}.

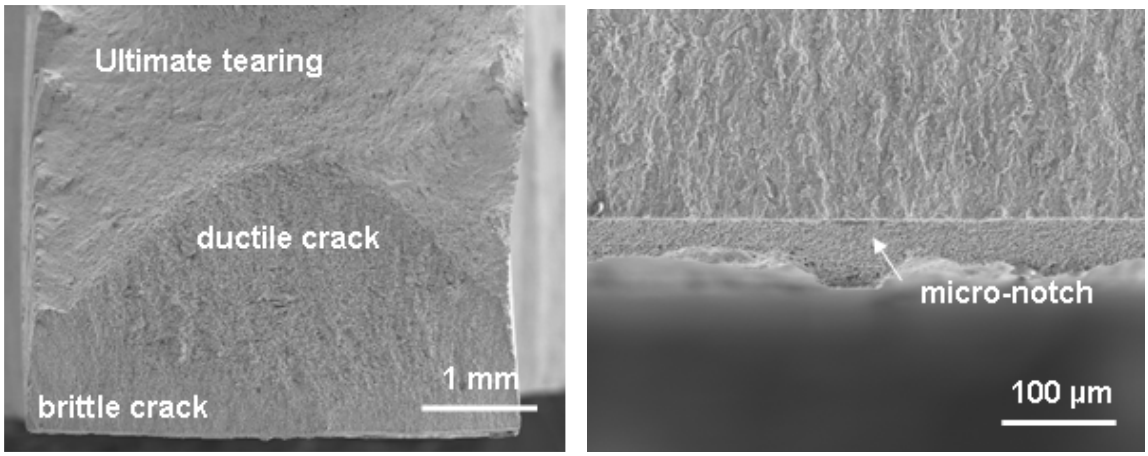

Figure 5: SEM fractographs of the steel A specimen tested at -1170mV/SCE in 3 wt% NaCl de-aerated solution and 10^{-6} s^{-1}, showing (a) general view at low magnification, (b) the region near the notch root with quasi-cleavage features in the propagation region.

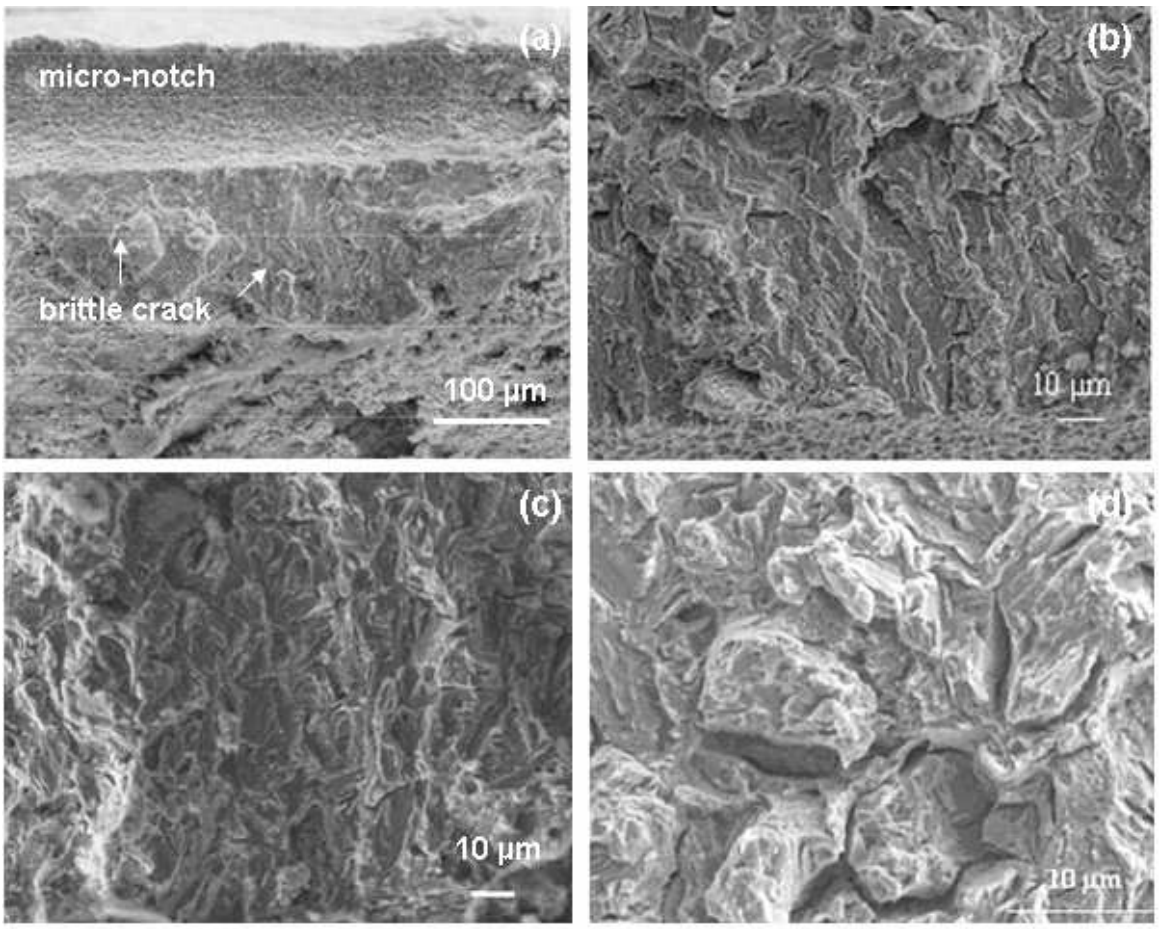

Figure 6: SEM fractographs of the steel B specimens tested at (a) -900 mV/SCE and 10^{-6} s^{-1}, (b) -900 mV/SCE and 10^{-7} s^{-1}, (c) -1170 mV/SCE and 10^{-6} s^{-1}, and (d) -1170 mV/SCE and 10^{-7} s^{-1}, in 3 wt% NaCl de-aerated solution.

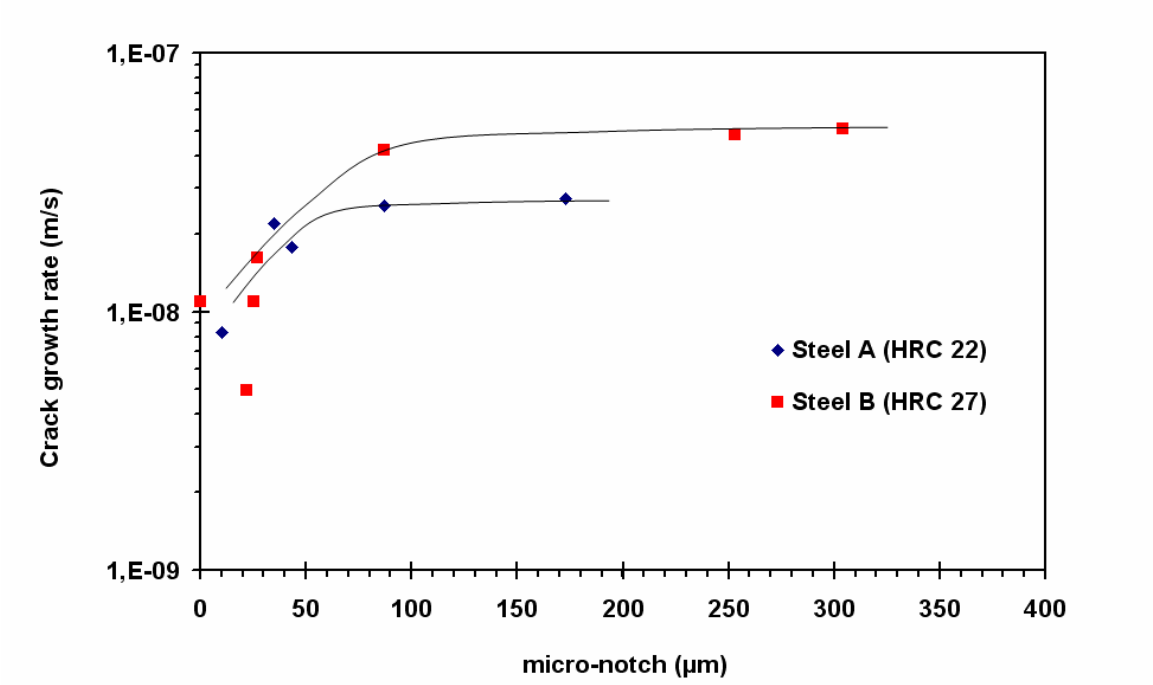

Figure 7: Plot of CGRs *vs* micro-notch depth during slow strain rate tests in 3 wt% NaCl de-aerated solution at Ec = -1170 mV/SCE and $\dot{\varepsilon} = 10^{-6}$ s^{-1} for steels A and B.

3.2 Low-amplitude cyclic tests

Figure 8 shows the crack growth rates *vs* maximum load applied relative to the yield stress of the steels, according to hydrogenation conditions. It is noted that in air, no propagation occurred for both steels in these cycling conditions, at least up to 90% of their yield stress. Similarly, tests with a stress ratio of 0.6 didn't show any crack initiation in NaCl solution at Ec = -1170 mV/SCE. The general shape of curves shows a strong effect of the applied stress on crack growth rates. Nevertheless, in low to moderate hydrogen activity conditions (open symbols), the CGRs of both steels are indistinct and seem to belong to the same scatter band. In these conditions, crack growth rates depend on the local plastic strain imposed by the loading rather than the microstructure of steels. On the contrary, when hydrogen activity was higher (closed symbols), the behaviour of the two steels are clearly distinct. Steel B appears more sensitive to hydrogen embrittlement than steel A, since its crack growth rates are higher by more than an order of magnitude whatever the level of loading, *ie* the local plastic strain. The results show also that to reach the same crack growth rate, steel A requires to be solicited at a higher plastic strain level. Moreover, the threshold of crack propagation for steel A is higher than steel B. Considering the absolute applied stress rather than the loading compared to the flow stress of steels, we found that both steels have a quite similar sensitivity to hydrogen embrittlement in these test conditions (Fig. 9), the slight difference could be link to their microstructure.

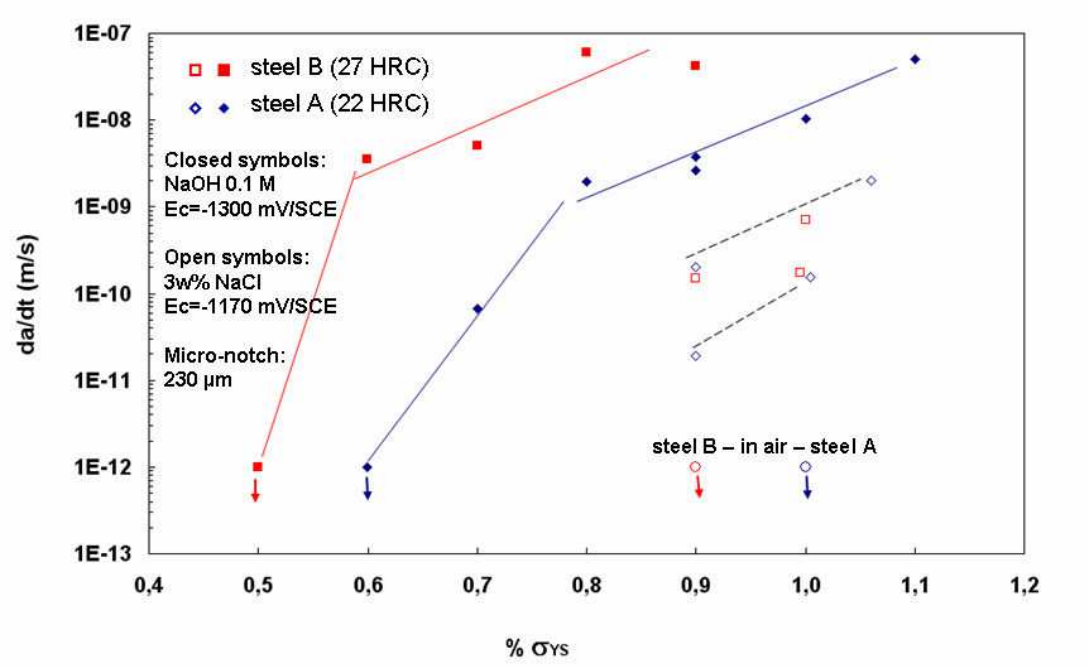

Figure 8: Plot of CGRs *vs* maximum stress applied relative to the YS of steels A and B, at R = 0.5 and 5.10^{-3} Hz, in moderate and high hydrogen activity conditions and in air.

Figure 10 shows typical fracture surfaces of the steel A and steel B specimens tested in the two hydrogenating conditions. The fracture mode was brittle in both cases, but when hydrogen activity was reduced (Fig. 10a and Fig. 10c), ductile tearing appeared and separated quasi-cleavage fracture plans, while in highly hydrogenating conditions, an intergranular and transgranular mixed mode prevailed the rupture of specimens.

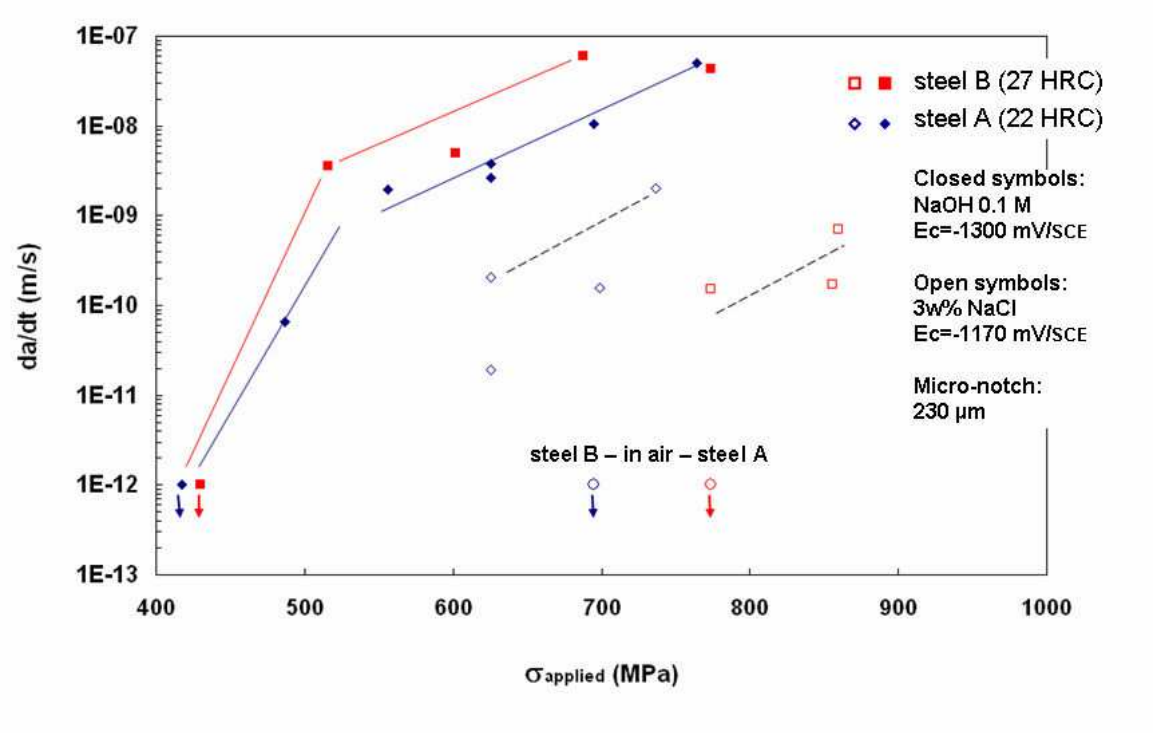

Figure 9: Plot of CGRs *vs* absolute maximum stress applied for steels A and B, at R = 0.5 and 5.10^{-3} Hz, in moderate and high hydrogen activity conditions and in air.

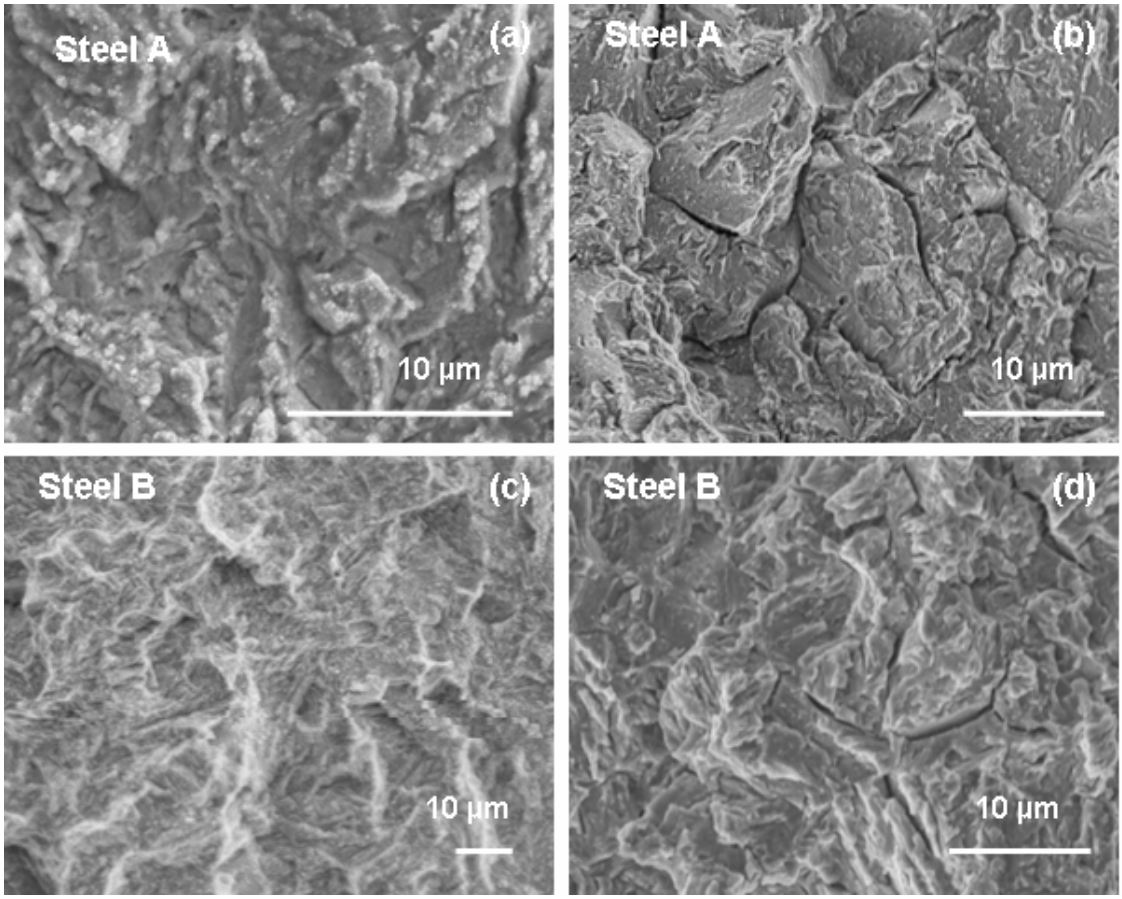

Figure 10: Low cycle fatigue tests SEM fractographs of the steel A specimens tested at (a) -1170 mV/SCE in NaCl solution, and (b) -1300 mV/SCE in NaOH solution, and the steel B specimens tested at (c) -1170 mV/SCE in NaCl solution, and (d) -1300 mV/SCE in NaOH solution.

4 Summary and conclusions

In this paper, we have presented experimental results from hydrogen embrittlement study of high strength low alloy steels. Slow strain rate tensile testing and low-amplitude cyclic testing on micro-notched specimens in various hydrogenation conditions and at various micro-notch depths were used to highlight the respective role of microstructure, local plasticity and hydrogen effects on the mechanism of hydrogen embrittlement.

During SSRTs, the higher crack growth rates were measured when strain rates and cathodic potentials were lowest and micro-notch depths greater. These results show that hydrogen embrittlement is enhanced when stress triaxiality and local plastic strain at notch tip are high. Moreover, static loading test results on steel A in highly hydrogenating conditions (NACE Standard Tensile Test TM0177-96) show that dynamic strain rate is required to embrittle the steel during cathodic charging. In these conditions, fracture surfaces show an IG and TG mixed mode of rupture, which is consistent with the literature, see for example Wang *et al.* [11]. The CGRs are then equal to 2.5 10^{-8} m/s for steel A and 5 10^{-8} m/s for steel B, which is twice higher and could reflect the intrinsic sensitivity difference between the microstructures.

Low-amplitude cyclic testing results showed that in highly hydrogenating conditions, crack growth rates depend mainly on the local stress rather than the plastic strain at notch tip. The slight difference between the two steels, a 2-3 ratio between the two CGRs, is presumably linked to their microstructure. In moderate hydrogenating conditions, local plastic strain at notch tip seems to prevail on the fracture process. In these conditions, CGRs between the two steels were quite similar and didn't depend on their microstructure.

5 References

[1] Hirth JP.
Metall Trans A 11A, pp 861, 1980.

[2] Turnbull A.
Modelling of environemental assisted cracking
Corrosion Science 34, pp 921-960, 1993.

[3] Gao H., Cao W., Fang C, Rios E.R. De Los
Analysis of crack tip hydrogen distribution under I/II mixed mode loads
Fatigue Fract. Eng. Mater. Struct. 17, pp 1213-1220, 1994.

[4] Green J.A.S., Hayden H.W., Montague W.G.
In Effect of Hydrogen on Behavior of Materials, A.W. Thompson and I.M. Bernstein Eds (AIME, New York), p 200, 1976.

[5] Swanson R.E., Thompson A.W., Bernstein I.M.
Metall. Trans. 17A, p1633, 1986.

[6] Maier H.J., Popp W., Kaesche H.
Effects of hydrogen on ductile fracture of a spheroidized low alloy steel.
Mater. Sci. Eng. A 191, pp 17-26, 1995.

[7] Takai K., Shoda H.
Lattice defect formation and degradation enhanced by hydrogen and strain of metals
In Effect of Hydrogen on Materials, B. Somerday, P. Sofronis, R. Jones, Ed (ASM International, Ohio), pp 195-202, 2009.

[8] Wang M.; Akiyama E.; Tsuzaki K.
Effect of hydrogen on the fracture behavior of high strength steel during slow strain rate test.
Corrosion Science 49, pp 4081-4097, 2007.

[9] Lee W.-S.; Su T.-T.
Mechanical properties and microstructural features of AISI 4340 high strength steel under quenched and tempered conditions.
Journal of Materials Processing Technology 87, pp 198-206, 1999.
[10] Peterson R.E.
Stress concentration Factors.
John Wiley and Son, New York, 1974.
[11] Wang M., Akiyama E., Tsuzaki K.
Effect of hydrogen on the fracture behavior of high strength steel during slow strain rate test.
Corrosion Science 49, pp 4081-4097, 2007.